Phonon-based scalable platform for chip-scale quantum computing

Charles M. Reinke¹ and Ihab El-Kady^{1,2,a}

¹Department of Applied Photonic Microsystems, Sandia National Laboratories, P.O. Box 8500 MS-1082, 87185, Albuquerque, USA

We present a scalable phononic crystal-based platform for observing the phonon analogy of cavity quantum electrodynamics, called phonodynamics, in a solid-state system. Practical schemes involve selective placement of a single acceptor atom in the peak of the strain field in a high-Q phononic crystal cavity that enables strong coupling of the phonon modes to the energy levels of the atom. We show theoretical optimization of the cavity design and excitation waveguide, along with estimated performance figures of the coupled system. Additionally, a qubit can be created in the same platform by entangling a phonon at the resonance frequency of the cavity with the atom states, but in the weak coupon regime. Qubits based on this half-sound, half-matter quasi-particle, called a phoniton, may outcompete other quantum architectures in terms of combined emission rate, coherence lifetime, and fabrication demands.

I. INTRODUCTION

Cavity quantum electrodynamics (QED) has become an important field of quantum mechanics research due to the inherent strong light-matter interactions. Additionally, circuit QED has developed as a stable, solid-state platform in which to investigate light-matter interactions, without the inconvenience of bulky macroscopic cavities as in the case of cavity QED. Most recently, the use of phonons in place of photons has led to research in cavity phonodynamics, which has the attractive feature of combining the advantages of cavity QED with a solid-state platform¹. Qubits based on

²Department of Electrical and Computer Engineering, University of New Mexico, Albuquerque, New Mexico 87131. USA

^aAuthor to whom correspondence should be addressed. Electronic mail: ielkady@sandia.gov.

this half-sound, half-matter quasi-particle, called a "phoniton", have been predicted to outperform quantum dot-based qubits and approach circuit QED performance in the MHz frequencies¹.

Current qubit implementations are limited by the tradeoff between coherence lifetime and Rabi frequency. For example, trapped ions have demonstrated coherence times on the order of several minutes, but have emission rates in the few kHz², while quantum dots are limited to short lifetimes due to dephasing times in the nanoseconds but have Rabi frequencies in the tens of MHz³. The phoniton approach avoids this tradeoff, allowing for predicted lifetimes in the milliseconds with MHz Rabi frequencies. This puts the phoniton on similar performance standing as circuit QED systems⁴, with the added advantage that the phonons act as "local" flying qubits. The phononic benefit is further amplified with ability to coherently convert them to photons for "distant" flying qubits using optomechanical transduction⁵. Phonons, due to their unique properties, enable new opportunities for quantum devices and physics. These properties include a solid-state environment, strong phonon-phonon interaction, relatively long coherent lifetimes, and strong coupling to lattice strain fields.

II. THE PHONITON UNDER STRONG COUPLING

In this paper, we study a phonon-based, solid-state analogue of the cavity QED system that requires the selective placement of a single acceptor atom, such as B, in the strain field peak of a high-Q phononic crystal (PnC) cavity fabricated in Si. A combination of background strain and an applied external magnetic field serves to remove the degeneracy and tune the energy levels of the atomic spin states to match the energy of the cavity resonance. These spin states can be used as a qubit with phonons employed to move from one state to another by flipping the spin of the acceptor impurity. Entangling a phonon in the cavity mode with the acceptor atom spin states enhances the coupling and thus increases the coupling rate. The inherent scalability

of this chip-scale system opens the door to the selective entanglement of large numbers of qubits, a necessary criterion for the implementation a practical quantum computer. Furthermore, successful demonstration of a phoniton will open the door for single phonon sources, an essential ingredient for phonon lasing⁶.

While the proposed phoniton system has many similarities with existing cavity QED devices that use quantum dots, it has the distinct advantage of indistinguishable single-atom qubits. Contrast this to the monodispersity issue in quantum dots and the impossibility of fabricating two identical Josephson junctions using even the best state-of-the-art techniques, necessitating the complication of incorporating a tuning mechanism. The inherent indistinguishability of these phonitons leads to higher entanglement rates for multiple qubits as compared to a comparable system that uses, for example, quantum dots⁷. Furthermore, the use of a solid-state qubit in an integrated platform eliminates the need for the sensitive alignment of laser beams necessary to set up an optical lattice atom trap, and also results in longer trap times (and hence a more stable qubit) than in the case of trapped ion systems, which suffer from random particle collisions that are present in even the highest achievable vacuum environment. Thus, deterministic, long-lifetime qubits can be engineered in a package that requires minimal maintenance once a closed-cycle cryogenic environment has been established. A further benefit of the proposed system, as with all cavity based qubit systems, is that the inevitable fabrication errors will only affect the cavity resonance width and quality factor. Bearing in mind that the atomic resonance width is negligibly small when compared to that of the cavity the highest impact of such errors is to only misalign cavity resonances and broaden the cavity peak (or possibly degrade the Q), but they will not affect the atomic states. Thus, the use of a high-Q cavity virtually guarantees qubit entanglement with high fidelity.

A. Acceptor Atom Quantum System

The 4-fold ground state degeneracy of the acceptor atom can be split by a combination of strain and applying an appropriate magnetic field, resulting in four states $|\phi_1\rangle = |-3/2\rangle$, $|\phi_2\rangle = |-1/2\rangle$, $|\phi_3\rangle = |1/2\rangle$, and $|\phi_4\rangle = |3/2\rangle$, that can be used to create a qubit¹. Incorporating the effects of strain into the Hamiltonian of the system results in a vacuum Rabi splitting frequency given by

$$g^{3/2,1/2} = d' \left(\frac{\hbar \omega_a}{8\rho \hbar^2 V v_t^2} \right)^{1/2}, \tag{1}$$

where d' is a renormalized deformation potential constant determined from experiment, ω_a is the angular frequency corresponding to the qubit splitting energy, ρ is the mass density of Si, V is the phononic mode volume in the PnC cavity, and v_t is the transverse sound velocity in Si. The bulk phonon emission rate can be calculated as

$$\Gamma = \frac{\omega_a^3}{10\pi\rho\hbar} d' \left(2/3v_l^5 + 1/v_t^5 \right), \tag{2}$$

where v_l is the longitudinal sound velocity in Si. Additionally, the average thermal phonon number can be calculated as

$$n_{th} = \frac{1}{e^{\hbar \omega / k_B T}},\tag{3}$$

where T is the temperature of the system. Combining these equations with the decay frequency of the cavity mode, $\kappa = \omega_a/Q$ where Q is the quality factor of the PnC cavity, results in the number of observable Rabi oscillations, given as

$$n_R = \frac{2g^{3/2,1/2}}{\Gamma + \kappa} \frac{1}{1 + 2n_{th}},\tag{4}$$

which provides an indication of the strength of the wave-matter coupling. It can be immediately deduced from these equations that the Q of the phononic crystal cavity should be as high as possible to achieve strong coupling or high entanglement rates. We thus start our analysis by

delving into an investigation of the optimal Q regime of operation. Figure 1 shows a plot of the anticipated number of Rabi oscillations for various qubits (different external magnetic field strengths) versus temperature for different Q regimes.

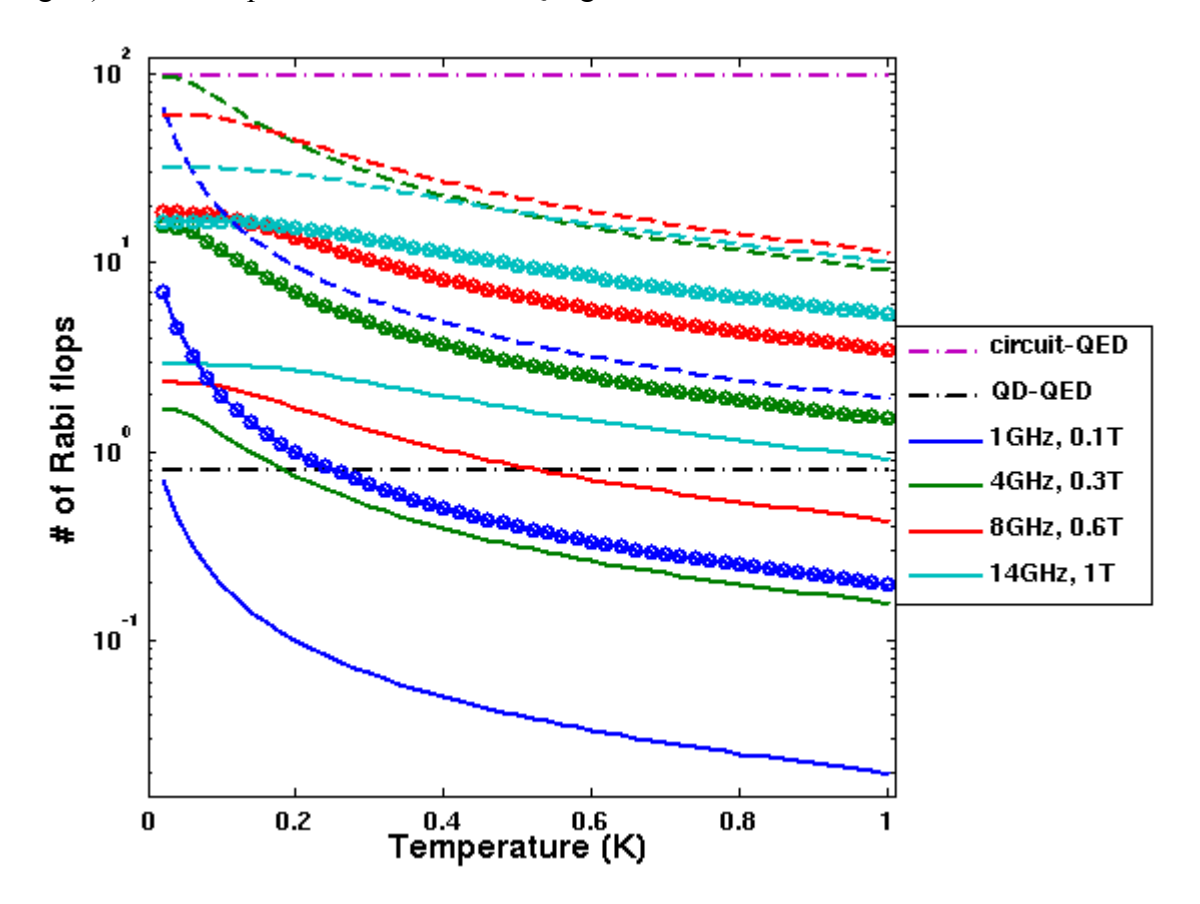


FIG. 1. Calculated number of Rabi flops of the phoniton system for various cavity resonance frequencies; solid lines indicate Q = 103, circles indicate Q = 104, and dashed lines indicate Q = 105. The number of Rabi flops for the QD-QED³ and circuit-QED⁴ systems are also shown for reference.

Clearly, Qs on the order of 1000 (indicated by solid lines) provide a very small number of Rabi flops, resulting in gate times that are uncomfortably close to the decoherence lifetime. On the other hand, while Q values larger than 10⁵ (dashed lines) would yield the highest flop rates, they would unfortunately require fabrication tolerances that cannot be obtained using state-of-the-art fabrication techniques, and at the frequencies of interest (few GHz) the excitations would exceed the maximum f·Q limit of Si⁸. However, Q values around 10⁴ (circles) are reliably obtainable and offer Rabi oscillation performance that exceeds the best quantum dot systems. Next, we

perform an analysis on the most practical temperature range of operation. Two ranges are identified: typical dilution fridge temperatures of about 20mK and temperatures achievable with a standard ³He cryostat of around 270mK. The performance metrics, such as cooperativity parameter, indicates that at dilution fridge temperatures (20mK) qubits with lower frequencies in the range of 1-4GHz perform best, as shown in Fig. 2, even matching or exceeding the best performance for circuit-QED systems, whereas at the lowest ³He cryostat temperatures (270mK) the optimal qubit frequencies are around 10GHz, as seen in Fig. 3. These atomic level splitting frequencies can be easily reached with superconducting electromagnets providing in excess of 1T magnetic fields.

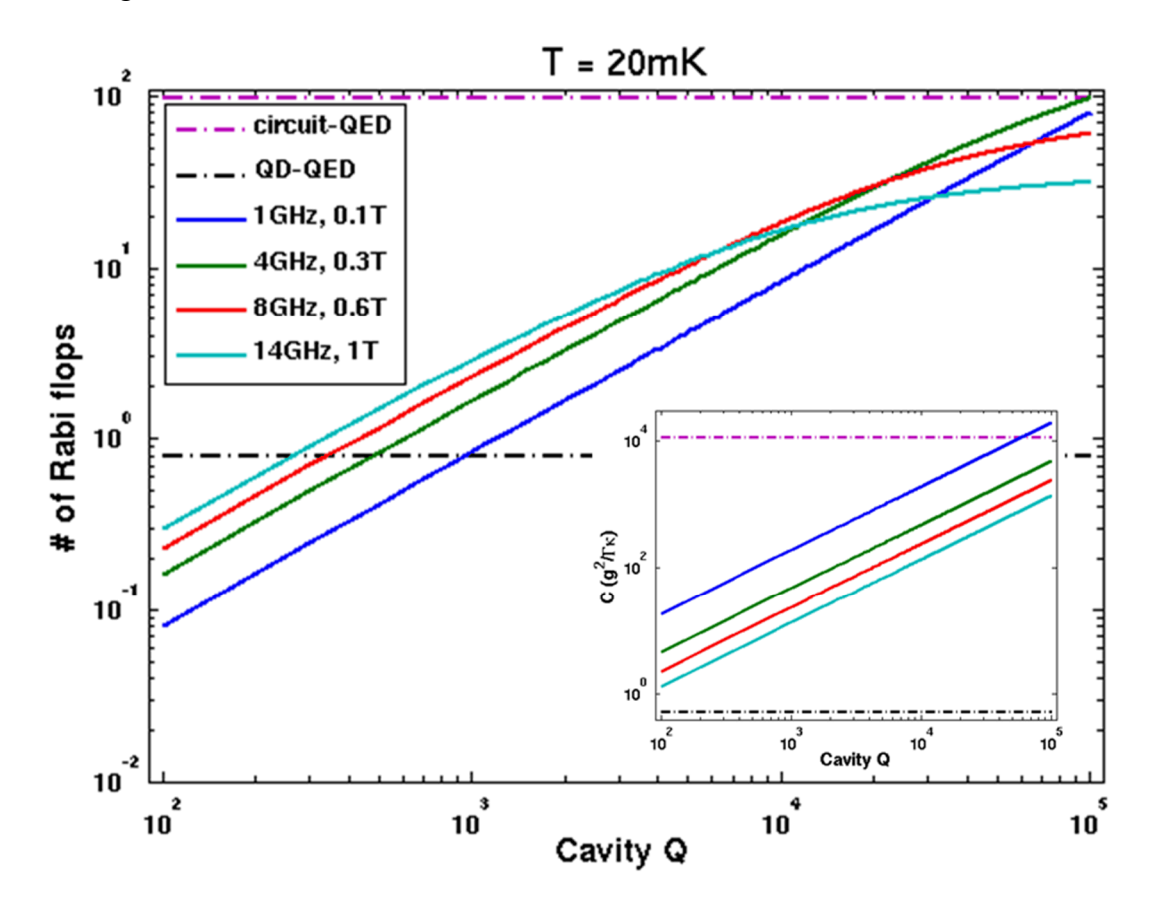


FIG. 2. Calculated number of Rabi flops at 20mK versus cavity Q for the 1GHz, 4GHz, 8GHz, and 14GHz qubits. Inset shows the cooperativity parameter of the phoniton system for the same parameters. The performance of the circuit-QED and QD-QED systems are also shown for reference.

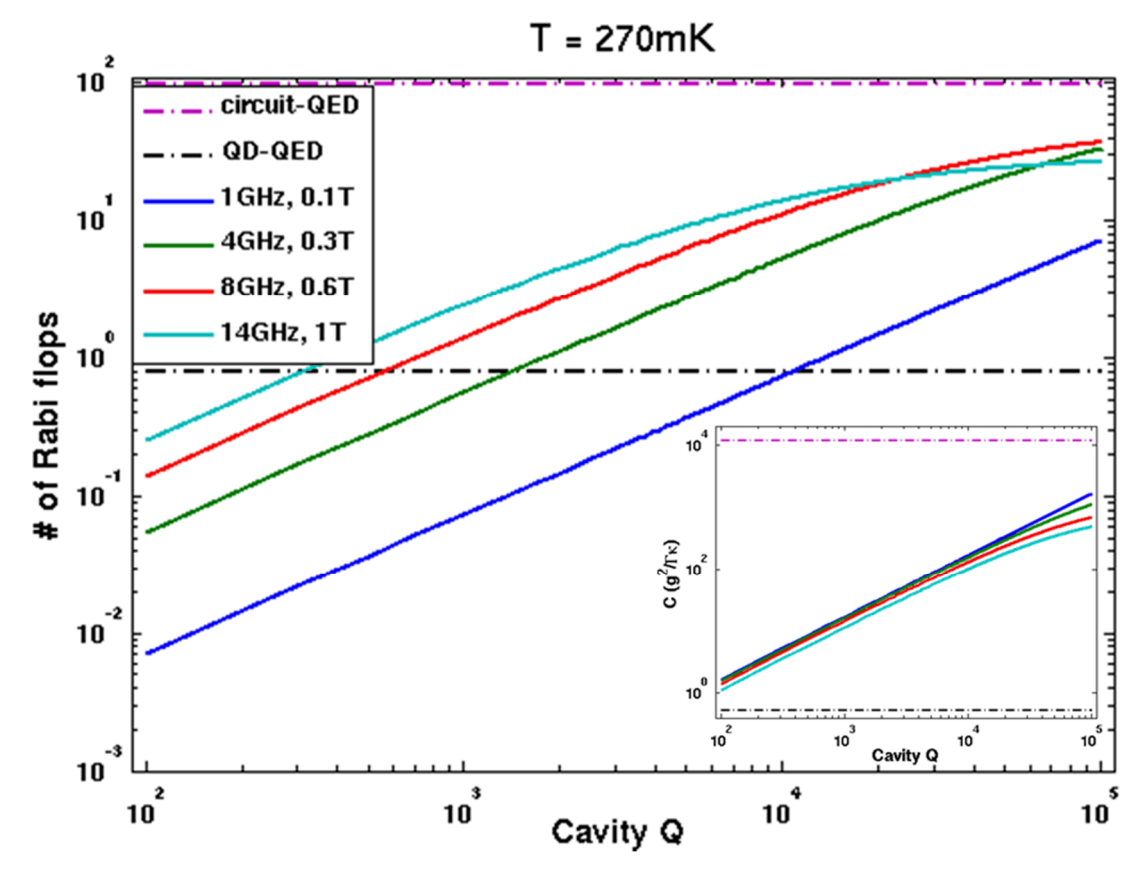


FIG. 3. Calculated number of Rabi flops at 270mK versus cavity Q for the 1GHz, 4GHz, 8GHz, and 14GHz qubits. Inset shows the cooperativity parameter of the phoniton system for the same parameters. The performance of the circuit-OED and OD-OED systems are also shown for reference.

The phoniton system is also attractive from a quantum computing perspective, as all of the DiVincenzo criteria⁹ can be adequately satisfied. The phoniton system presented here is based on a scalable, solid-state architecture (planar PnCs), which address the need for well-characterized qubits and system scalability. The manipulation of qubits using well-understood RF phononics enables the initialization of the qubit state and the realization of a universal set of quantum gates. Since the qubits are based on electronic states in identical single atoms, the gate operation times can easily be made shorter than the qubit coherence times and multiple qubits can be entangled without the need for frequency conversion or tuning. Moreover, by using AlN transducers or optomechanical conversion, single-qubit states readout can be achieved in a straightforward manner. Lastly, since phonons can be used as "local" flying qubits and

converted to "global" flying qubits (photons) with optomechanical devices, stationary qubits can be converted into flying qubits, providing for high-fidelity long-distance transmission of qubits.

B. Selective Atom Placement

One of the largest hurdles in implementing this phoniton scheme is the selective placement of a single atom in the PnC cavity, which is necessary for optimal performance since the acceptor atom should ideally be in the highest-strain region of the resonator. Single-atom implantation has been demonstrated previously¹⁰, although with finite straggle parameters that require a suitably large target for implantation. The ability to selectively place a single atom sets this work apart from others in this field that instead rely on randomly distributed defect atoms in high-purity Si, necessitating the fabrication of large numbers of devices in the hopes finding at least one that has the desired single atom placement. The selective implantation of a single atom would be performed using an ion implantation system, with carefully controlled beam currents and photolithography masks used to maximize the probability of implanting only one atom in the desired location. Nevertheless, there will still be some straggle in the final position of the atom due to a finite beam width and the unpredictable path the atom will take one it impacts the Si lattice. Based on previous research, the straggle can be estimated to that correspond to a placement uncertainty of ± 65 nm in the lateral (in-plane) dimensions and ± 90 nm in depth¹¹. These values place constraints on the minimum thickness that the PnC slab can be and also on the topology of the PnC cavity, since the engineered cavity mode must have a high-strain region that is at least as large as the in-plane straggle to guarantee that the implanted atom can be excited.

Earlier work¹ had proposed the use of two types of PnC designs for practical realization of a phoniton. These structures were chosen based on their eventual potential for optomechanical

application, as they act as both photonic and phononic crystals. The first was the ladder-type 1D crystal, which has a demonstrated Q value exceeding 10⁴ combined with strong confinement of phonons in the cavity¹². However, the elastic waves in this design were excited using optomechanical coupling to the evanescent field of a tapered optical fiber, a technique known for being tedious to assemble. Additionally, the reported high-Q performance of the cavity is based on a calculated intrinsic Q of a separate phononic cavity; the actual observed Q of the optomechanical device was only on the order of a few hundred. To address this issue, high-Q phononic crystal cavities have been designed with strain field distributions large enough to accommodate the single-atom placement straggle limits imposed by state-of-art FIB technology. Thus, a second design was considered for this work, namely the "snowflake" air hole PnC in a Si membrane, which has been theoretically shown to exhibit both a photonic and a phononic bandgap for in-plane propagating modes⁵. The original optomechanical cavity design based on this lattice entailed the simple removal of two "snowflake" air holes, but the peaks of the strain field for the mechanical cavity mode were isolated to the corners of the geometry, with in-plane dimensions that were smaller than the corresponding straggle in atom placement, mentioned earlier. Optimization over several cavity topologies to drawn the strain field into a broader topology resulted in a design created by removing two adjacent inclusions and the "arms" of the surrounding inclusions to create a smooth area, as shown in Fig. 4(a). This phononic cavity had a lattice constant of 400nm, slab thickness of 160nm, snowflake radius of 168nm, and a snowflake arm width of 60nm. The resulting theoretical mechanical Q factor is greater than 5·10⁴ (Fig. 4(b)), with two high-strain field lobes that are uniform over approximately 200nm and separated by a zero-strain node, as seen in Fig. 4(c). Either of these lobes would easily encompasses the straggle parameters of the atom implantation. Cross-sections of the strain field

in various positions through the peaks of the cavity in all three dimensions, as shown in Fig. 5, clearly indicate that the regions of maximum strain are broad, alleviating the fabrication and single-atom placement constraints of the cavity.

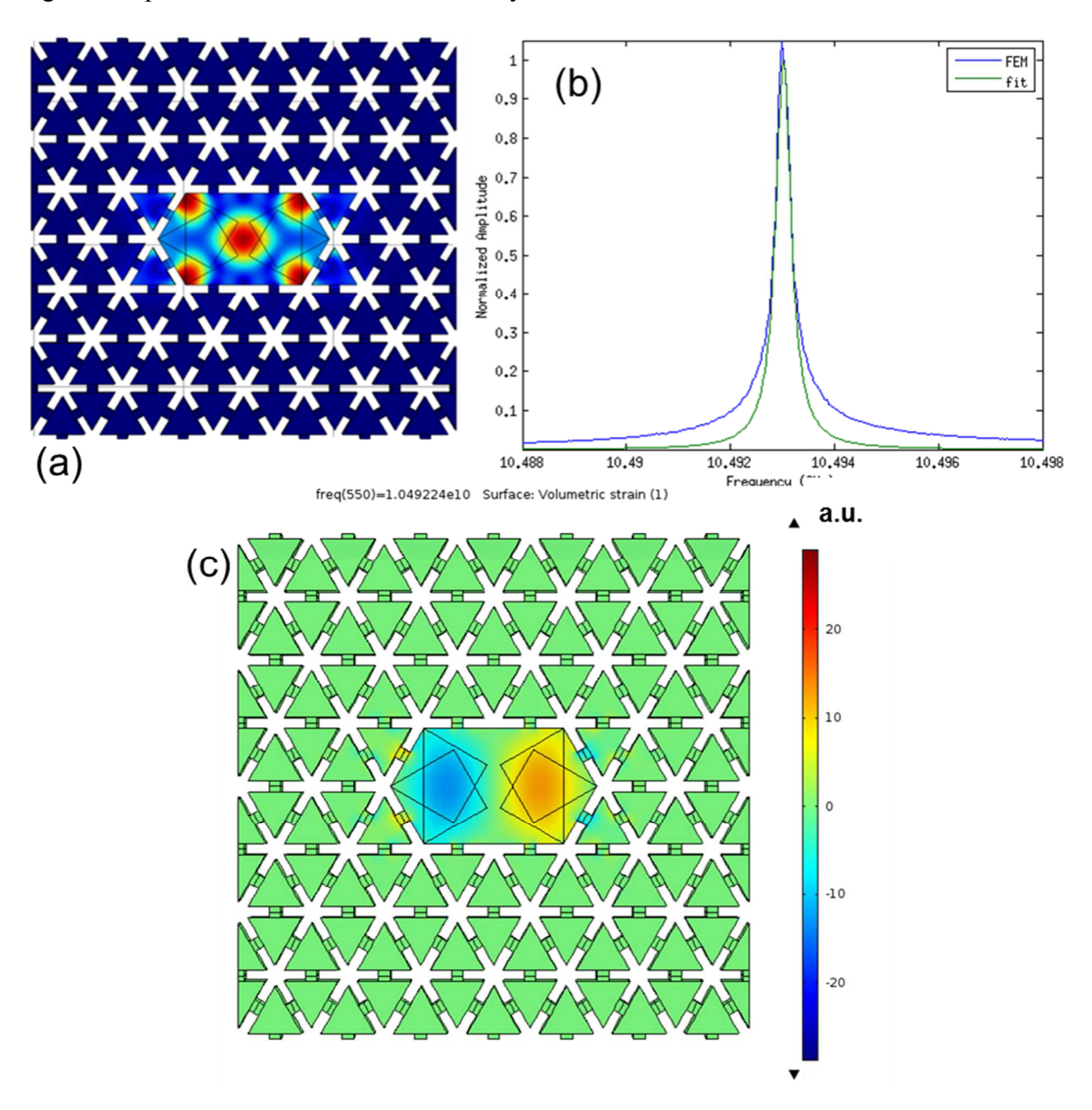


FIG. 4. (a) Calculated displacement field of the optimized phononic cavity. (b) Calculated frequency response of the cavity; the Lorentzian fit indicates a Q of greater than $5 \cdot 10^4$. (c) Calculated strain field of the cavity.

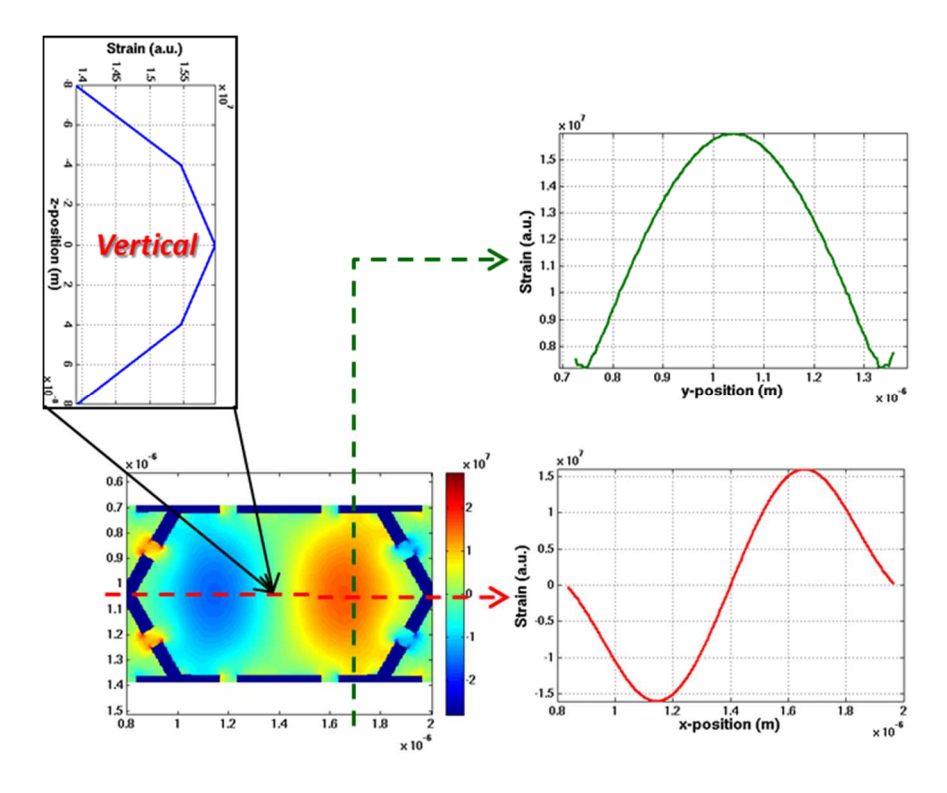


FIG. 5. Calculated strain field of the optimized phononic cavity shown in Figure 4(a), showing the profile along various cuts through the geometry.

III. PHONITON QUBIT

A. Phoniton Lifetime

We can also examine the phoniton qubit in the weak coupling regime and estimate the timescale for an entanglement event by a cavity QED analysis which will determine the lim its to overall speed of an entangled network. Here, we can look at two cases, a) where the cavities are coupled b) where the cavities are decoupled. Both timescales are relevant to a quantum computing architecture, where some of the information exchange will be local and some will be remote. In the case where the cavities are coupled and using equations borrowed from cavity QED with photons, we can calculate the Purcell enhancement as $2C+1^{13, 14}$, where C is the coopertivity factor $g^2/(2\kappa\gamma)$, g is given by Eq. (1), and γ is the spontaneous emission rate of the acceptor. Using values consistent with this paper, $d^2 = -3.7\text{eV}$ for boron¹, v_l in silicon is 8990m/s, v_l is 5288 m/s, and cavity volumes of $5.8\cdot10^{-18}$, $3.64\cdot10^{-19}$, $9.10\cdot10^{-20}$, and $2.97\cdot10^{-20}$ m³,

these equations yield Purcell factors of approximately 3000, 950, 500, and 300 for the 1, 4, 8, and 14GHz designs, respectively. Related to the Purcell enhancement is the β factor that describes the fraction of photons emitted into the cavity mode and can be given as 2C/(2C+1), which is 0.9997, 0.9990, 0.9980, and 0.9964 for the four respective qubit designs. Multiplying by the bulk phonon emission rate calculated in Eq. (2), we can expect enhanced spontaneous emission ranging from 1.5 to 350MHz depending on the mode volume.

Assuming a phonon propagation time of a few nanoseconds between cavities, we can expect an entanglement event on average in less than a microsecond, and perhaps on the order of tens of nanoseconds. If the cavities are not directly coupled, there are additional losses coupling to a waveguide, propagating through the waveguide, and coupling to a second cavity that will slow the rate of entanglement, depending on the distance between cavities. The loss coefficient can be calculated as $\alpha = \omega_a/(2\nu_l Q)$, which assuming $\omega_a = 2\pi \times 10^9 \text{Hz}$ and $Q = 5 \cdot 10^4$ gives $\alpha = 74.5$ = 0.19dB/cm. For comparison, the propagation loss can be calculated for results recently published on a PnC waveguide-based resonator¹⁵ on another on a W2 PnC waveguide¹⁶. In the former case, $\omega = 2\pi \times 134.1418 \cdot 10^6$ Hz and the reported Q in air was 13500, giving an α of 3.70 = 0.06 dB/cm. In the latter work, the width of the resonance $\Delta \omega$ was about $4 \cdot 10^5 Hz$ (ω was about $2\pi \times 68 \cdot 10^6$ Hz), giving an α of 149.6 = 0.22dB/cm. Both of these values correspond well with what was estimated for the PnC design in the present case. In the case of the phoniton, it would also be necessary to consider the phonon shape as it is emitted into the waveguide and how likely that shape will be absorbed by the second cavity. Thus, this scheme will slow entanglement due to losses, but not impact fidelity, as entanglement could theoretically be heralded by probing with photons. Additionally, research has shown that exciting the cavity-atom system with an appropriately-shaped pulse can re-shape the phonon emitted from the cavity, mitigating this

issue¹⁷. Nevertheless, it is generally preferable to have coupled cavities where the coupling can be controlled and entanglement can be passed long distances by pairwise interactions.

Previous literature on the phoniton system included an additional problem that centers on the photon-phonon translator that was considered necessary for practical demonstration of the system^{1, 5}. This conversion introduces further difficulty into an already complicated system that is to be demonstrated for the first time. In fact, the photon-phonon translator that was proposed required two photonic waveguides, two phononic waveguides, and two precisely-tuned optomechanical cavities, all working together perfectly. Even if a simpler translator design could be used, optical access to a device in a cryogenic cooler is often unavailable and even when available optical focusing and alignment between the access window and the device is prohibitive. Thus, an electromechanical transduction scheme is advocated here that uses electrical excitation employing piezoelectric AlN transducers¹⁸, eliminating the requirement of optomechanical transduction. Conveniently, this electromechanical transduction scheme is well-suited to the dual requirements of high magnetic fields (a few Tesla) and low temperatures (mK) necessary for the observation of the phoniton.

B. Phoniton Qubit Neworks

To allow for entanglement among multiple qubits, a way of communicating between neighboring cavities is necessary. Thus, a waveguide was designed by creating a line defect of snowflakes with a radius reduced to 148nm, as shown in Fig. 6(a). The calculated waveguide dispersion behavior is shown in Fig. 6(b), where a single guided mode can be seen to intersect with the resonant cavity mode, shown in red. Three different cases of coupling between the waveguide and cavityhave been calculated: over-coupled at a separation of 1 lattice period (Fig. 7(a)), close to critically coupled at a separation of 2 lattice periods (Fig. 7(b)), and under-coupled at a separation of 3 lattice periods (Fig. 7(c)). The predicted Q drops slightly in the critically-

coupled case, as expected, to about $5.45 \cdot 10^4$, which is still within the range of greater than 10^4 required for strong coupling.

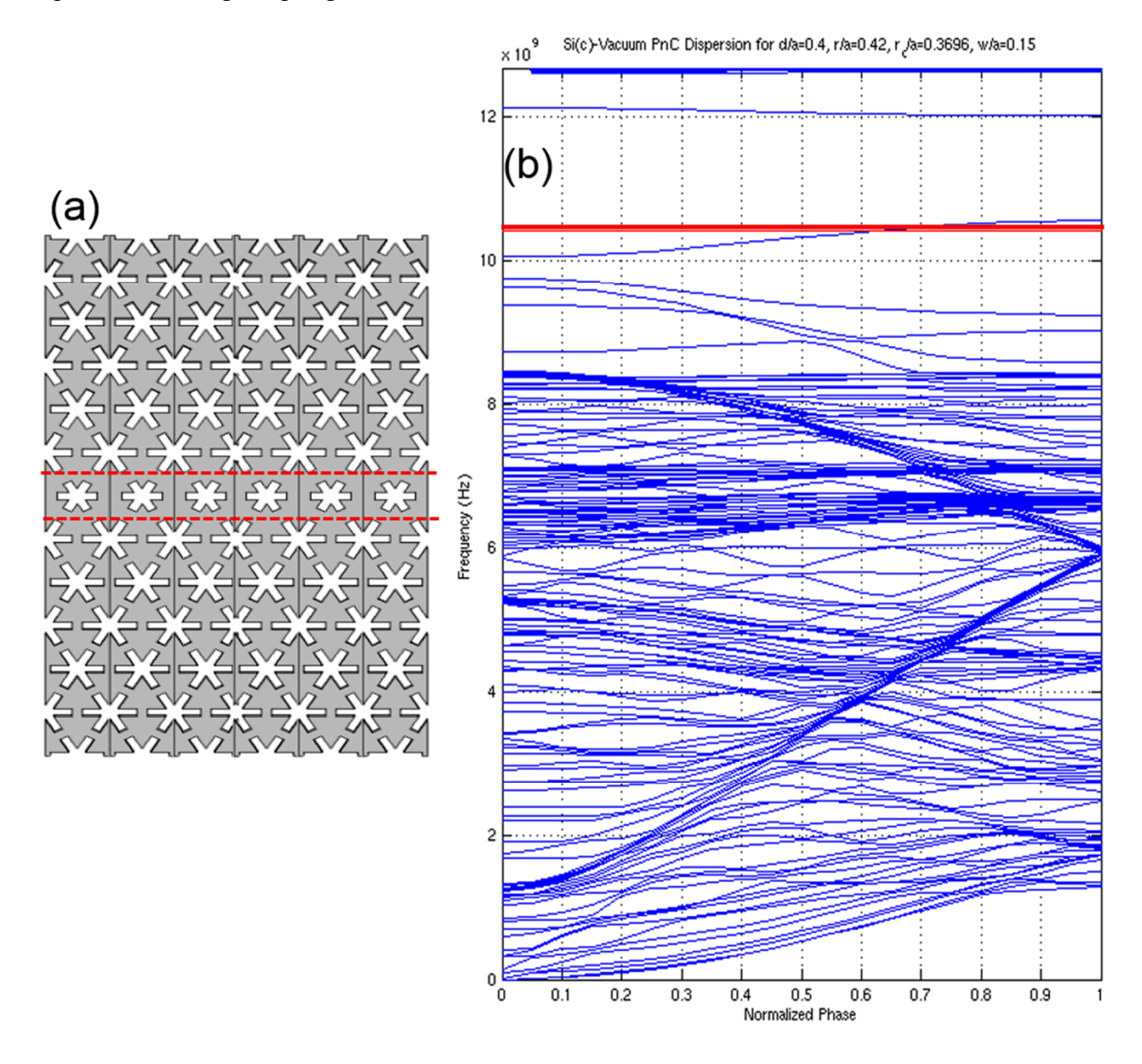


FIG. 6. (a) Phononic crystal waveguide design created by decreasing the radius of the snowflake inclusions by 20nm. (b) Calculated dispersion of the PnC waveguide with a single guided mode intersecting the resonant cavity mode, indicated in red.

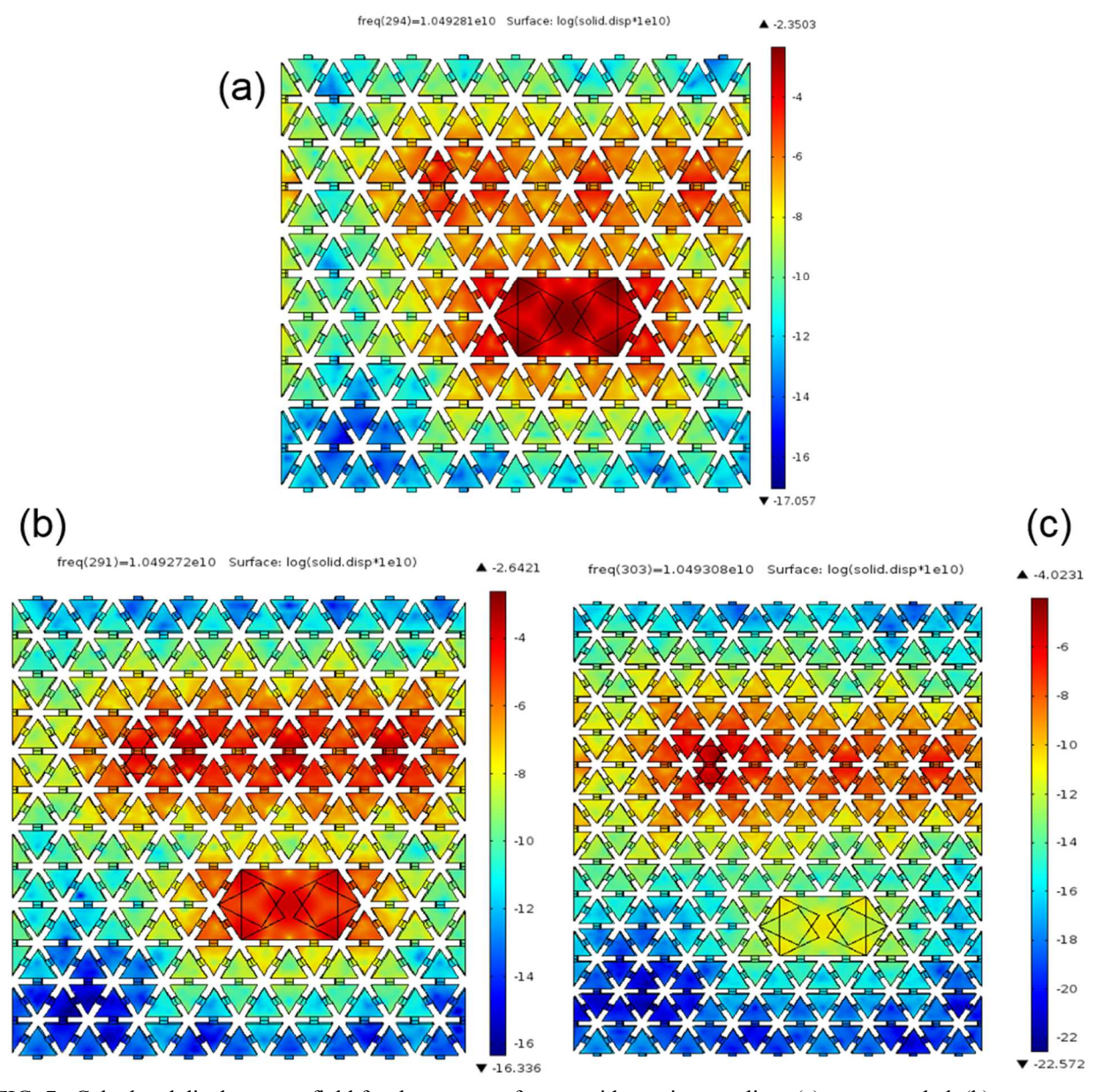


FIG. 7. Calculated displacement field for three cases of waveguide-cavity coupling: (a) over-coupled, (b) approximately critically coupled, and (c) under-coupled.

C. Phoniton Entanglement

An algorithm for entangling two neighboring qubits is required that preserved the quantum states of the atoms to be entangled. Figure 8(a) shows a schematic of a two-qubit system consisting of two phononic crystal cavities (A and B) each containing a single acceptor B-atom and coupled to a PnC waveguide. The process, shown in Fig. 8(b), begins with cooling

of the system (3 He Temp), forcing the atoms to the ground state. Next, a global microwave $\pi/2$ microwave pulse (black), whose frequency lies outside the PnC gap but supported by the lattice, is used to excite atoms A and B to an equal superposition of the -1/2 and +3/2 states. Then, a local microwave pulse (yellow) applied to atom A renders it in an equal superposition of the -3/2 and +1/2 states. Finally, atom A decays via path A4a (red) or A4b (blue), as shown in Fig. 8(b), by spontaneously emitting a phonon into the waveguide that is absorbed by the atom in cavity B. The results is that atoms A and B are now in a non-separable entangled state. This algorithm can be used to successively entangle adjacent qubits to link even far-spaced cavities and perform complex quantum computing operations.

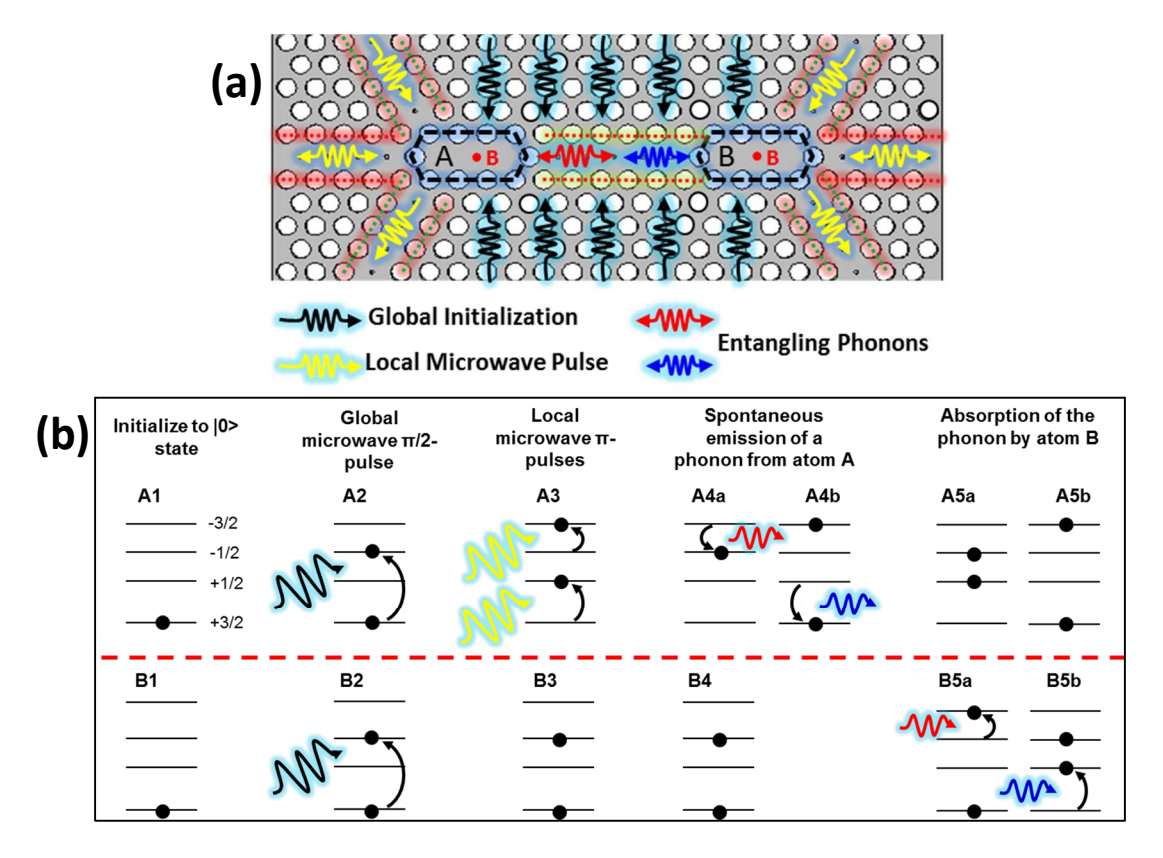


FIG. 8. (a) Schematic of a 2-qubit phoniton system. (b) Schematic of the proposed entanglement scheme.

D. Phoniton Scalability

This PnC platform and entanglement scheme enables us to directly scale up the number of interconnected qubits by creating a superlattice of resonantly coupled PnC-cavities and waveguides, as shown schematically in Fig. 9(a). To preserve the Q of individual cavities, a minimum separation (entangling waveguide length) of approximately 100 µm would be required. This sets an upper limit on the maximum number of possibly entangled qubits per unit area, as illustrated in Fig. 9(b).

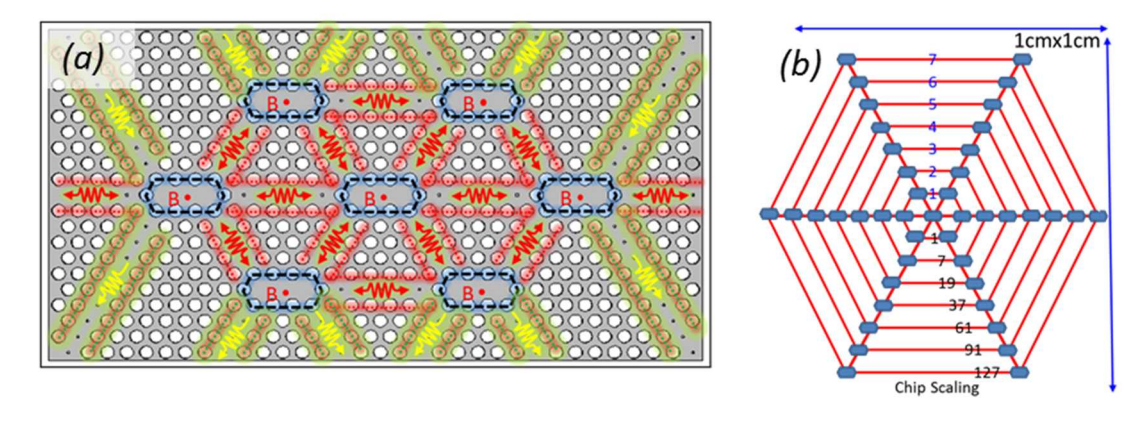


FIG. 9. (a) Schematic of possible system scale-up via coupled PnC cavities. (b) Estimated 127/cm² coupled qubits per PnC chip, assuming 100μm minimum separation between cavities.

An additional consideration is that although optomechanical transduction may ultimately be the most appropriate for quantum communication applications where there is a need for photons to carry qubit entanglement for long-distance communication, the optomechanical scheme introduces an additional complexity into the system that is not directly related to the phoniton concept, and also may be difficult to implement in the environment of a cryogenic cooler where impractical optical alignment issues would be imposed. Thus, to facilitate the realization of a practical phoniton system, we propose the electromechanical transduction scheme shown in Fig. 10. Electromechanical transduction of phonons at frequencies in excess of 2GHz at room temperature has been previously demonstrated using AlN interdigitated transducers deposited on Si¹⁸.

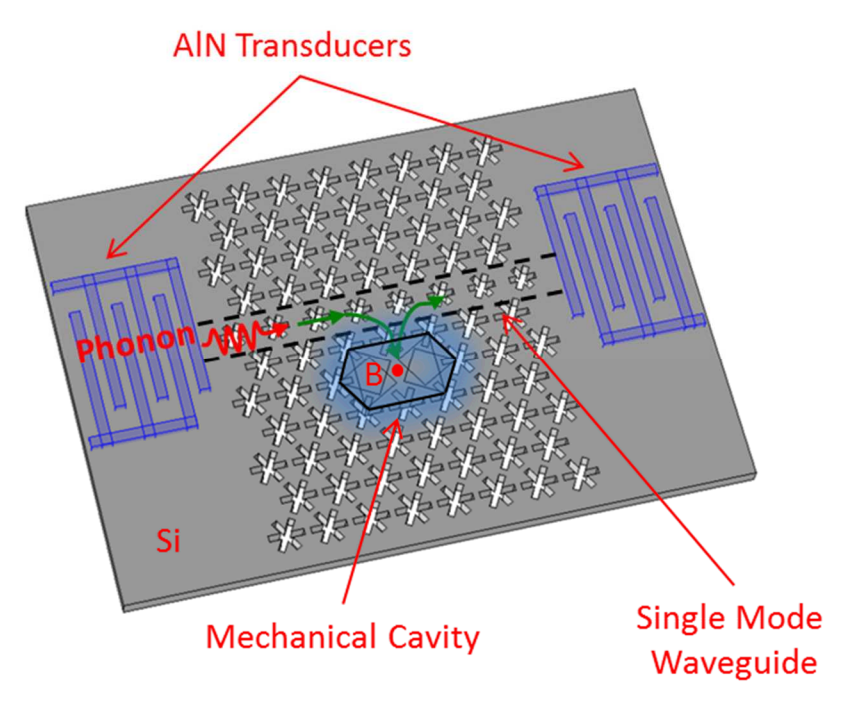


FIG. 10. Conceptual schematic of a cavity coupled to a waveguide with interdigitated transducers at either end of the waveguide for excitation and detection.

In this application, the simpler electrical transduction scheme circumvents the problem of optical access, as electrical feedthroughs are routinely used in cryogenic chambers and the test chip can be wire-bonded using materials that are matched in their coefficients of thermal expansion. In addition, measurements as low as 4K on AlN indicate that its performance will actually improve at cryogenic temperatures its due to improved intrinsic material Q ^{19, 20}, adding confidence that phononic operation up to 10GHz should be feasible.

IV. SUMMARY

In conclusion, we have presented the design of a chip-scale phononic crystal-based phoniton system, using waveguides and high-Q cavities operating in the 10GHz regime. This design in conjunction with a single acceptor atom implanted into the cavity forms the basis for a phonon-based qubit. Due to the high Purcell factor of this atom-cavity system, the qubit

performance generally exceeds that of quantum dots and approaches that of circuit-QED systems, while guaranteeing indistinguishability of the qubits. Moreover, the planar layout of the PnC makes it amenable to integration of multiple cavities and qubits, make the possibility of entangling record numbers of qubits within reach and the phoniton a promising technology for the realization of a practical quantum computer.

ACKNOWLEDGMENTS

The authors would like to thank Susan Clark and Edward Bielejec for enlightening discussions regarding qubit design and ion implantation. Sandia National Laboratories is a multi-mission laboratory managed and operated by Sandia Corporation, a wholly owned subsidiary of Lockheed Martin Corporation, for the U.S. Department of Energy's National Nuclear Security Administration under contract DE-AC04-94AL85000.

REFERENCES

- 1. R. Ruskov and C. Tahan, Physical Review B **88** (6), 064308 (2013).
- 2. S. Olmschenk, K. C. Younge, D. L. Moehring, D. N. Matsukevich, P. Maunz and C. Monroe, Physical Review A **76** (5), 052314 (2007).
- 3. R. Bose, D. Sridharan, H. Kim, G. S. Solomon and E. Waks, Phys. Rev. Lett. 108 (22), 227402 (2012).
- 4. D. I. Schuster, A. A. Houck, J. A. Schreier, A. Wallraff, J. M. Gambetta, A. Blais, L. Frunzio, J. Majer, B. Johnson, M. H. Devoret, S. M. Girvin and R. J. Schoelkopf, Nature **445** (7127), 515-518 (2007).
- 5. H. S.-N. Amir and P. Oskar, New Journal of Physics **13** (1), 013017 (2011).
- 6. I. Mahboob, K. Nishiguchi, A. Fujiwara and H. Yamaguchi, Phys. Rev. Lett. 110 (12), 127202 (2013).
- 7. R. Hafenbrak, S. M. Ulrich, P. Michler, L. Wang, A. Rastelli and O. G. Schmidt, New Journal of Physics **9** (9), 315 (2007).
- 8. D. Goettler, M. Su, Z. Leseman, Y. Soliman, R. Olsson and I. El-Kady, J. Appl. Phys. **108** (8), 084505 (2010).
- 9. D. Loss and D. P. DiVincenzo, Physical Review A 57 (1), 120-126 (1998).
- 10. M. J. Devlin, S. R. Dicker, J. Klein and M. P. Supanich, Cryogenics 44 (9), 611-616 (2004).
- 11. E. Bielejec, N. Bishop, and M. S. Carroll, presented at 2013 MRS Spring Meeting & Exhibit, San Francisco, CA (2013).
- 12. M. Eichenfield, R. Camacho, J. Chan, K. J. Vahala and O. Painter, Nature **459** (7246), 550-555 (2009).
- 13. A. B. Mundt, A. Kreuter, C. Becher, D. Leibfried, J. Eschner, F. Schmidt-Kaler and R. Blatt, Phys. Rev. Lett. **89** (10), 103001 (2002).
- 14. H. J. Kimble, Q. A. Turchette, N. P. Georgiades, C. J. Hood, W. Lange, H. Mabuchi, E. S. Polzik and D. W. Vernooy, in *Coherence and Quantum Optics VII: Proceedings of the Seventh Rochester Conference on Coherence and Quantum Optics, held at the University of Rochester, June 7–10, 1995*, edited by J. H. Eberly, L. Mandel and E. Wolf (Springer US, Boston, MA, 1996), pp. 203-210.

- 15. S. Mohammadi and A. Adibi, Microelectromechanical Systems, Journal of 21 (2), 379-384 (2012).
- R. H. Olsson, III and I. El-Kady, Meas. Sci. Technol. 20 (1), 012002 (012013 pp.) (2009). 16.
- L. M. Duan, A. Kuzmich and H. J. Kimble, Physical Review A **67** (3), 032305 (2003). 17.
- M. Ziaei-Moayyed, M. F. Su, C. Reinke, I. F. El-Kady and R. H. Olsson, III, 2011 IEEE 24th International 18. Conference on Micro Electro Mechanical Systems (MEMS 2011), 1377-1381 (2011).

 19. A. N. Cleland, M. Pophristic and I. Ferguson, Appl. Phys. Lett. **79** (13), 2070-2072 (2001).
- 20. C. Tu and J. E. Y. Lee, Sensors and Actuators A: Physical 244, 15-23 (2016).